Biomedicine & Pharmacotherapy 168 (2023) 115660

Contents lists available at ScienceDirect

Biomedicine & Pharmacotherapy

journal homepage: www.elsevier.com/locate/biopha

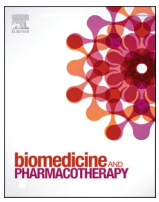

Inhibition of MD2 by natural product-drived JM-9 attenuates renal inflammation and diabetic nephropathy in mice

Minxiu Wang [a,b], Qianhui Zhang [a,b], Shuaijie Lou [b], Leiming Jin [b,c], Gaojun Wu [d], Wenqi Wu [b], Qidong Tang [b], Yi Wang [b], Xiaohong Long [b], Ping Huang [a], Wu Luo [a,d], Guang Liang [a,b,c,*]

[a] Department of Pharmacy and Institute of Inflammation, Zhejiang Provincial People's Hospital, Affiliated People's Hospital, Hangzhou Medical College, Hangzhou, Zhejiang 310014, China
[b] Chemical Biology Research Center, School of Pharmaceutical Sciences, Wenzhou Medical University, Wenzhou, Zhejiang 325035, China
[c] School of Pharmaceutical Sciences, Hangzhou Medical College, Hangzhou, Zhejiang 311399, China
[d] Department of Cardiology, the First Affiliated Hospital of Wenzhou Medical University, Wenzhou, Zhejiang 325035, China

ARTICLE INFO

Keywords:
Diabetic kidney disease
JM-9
Inflammation
Macrophage
Myeloid differentiation 2

ABSTRACT

Diabetic kidney disease (DKD) is one of the severe complications of diabetes mellitus-related microvascular lesions, which remains the leading cause of end-stage kidney disease. The genesis and development of DKD is closely related to inflammation. Myeloid differentiation 2 (MD2) mediates hyperlyciemia-induced renal inflammation and DKD development and is considered as a potential therapeutic target of DKD. Here, we identified a new small-molecule MD2 inhibitor, JM-9. *In vitro*, JM-9 suppressed high glucose (HG) and palmitic acid (PA)-induced inflammation in MPMs, accompanied by inhibition of MD2 activation and the downstream TLR4/MyD88-MAPKs/NFκB pro-inflammatory signaling pathway. Macrophage-derived factors increased the fibrotic and inflammatory responses in renal tubular epithelial cells, which were inhibited by treating macrophages with JM-9. Then, we investigated the therapeutic effects against DKD in streptozotocin-induced type 1 diabetes mellitus (T1DM) and type 2 diabetes mellitus (T2DM) mouse models. Treatment with JM-9 prevented renal inflammation, fibrosis, and dysfunction by targeting MD2 in both T1DM and T2DM models. Our results show that JM-9, a new small-molecule MD2 inhibitor, protects against DKD by targeting MD2 and inhibiting MD2-mediated inflammation. In summary, JM-9 is a potential therapeutic agent for DKD.

1. Introduction

Diabetic kidney disease (DKD) refers to a chronic complication of type 2 diabetes mellitus (T2DM) and and type 1 diabetes mellitus (T1DM) that impacts the kidneys [1]. Globally, DKD primarily contributes to the end-stage renal failure, which imposes a great financial burden to the society [2]. Physiologically, DKD gradually develops when hyperglycemia sets in, starting with mild renal inflammation and progressing to renal fibrosis and renal sclerosis, and finally leading to end-stage renal disease (ESRD). The primary risk factors encompass hypertension, hyperglycemia and genetic predisposition [3]. Hyperglycemia is the main aetiological factor for DKD [4] as it leads to metabolic changes that contribute to its development. Renin-angiotensin system inhibitors (RASIs) are the main therapeutic agents, however, there is still a significant risk of DKD onset and progression. Hence, new drugs shall be developed urgently to improve the health outcomes for patients suffering from this condition.

Chronic inflammation induced by hyperglycemia is a key

Abbreviations: BUN, blood urea nitrogen; BSA, bovine serum albumin; CMC-Na, carboxyl methyl cellulose; COL4, Collagen Type IV; DAB, diaminobenzidine; DAPI, 4',6-diamidino-2-phenylindole; DKD, diabetic kidney disease; ddH2O, double distilled water; DMEM, Dulbecco's Modified Eagle Medium; DMSO, dimethyl sulfoxide; ESRD, ultimately end-stage renal disease; FBS, fetal bovine serum; GAPDH, glyceraldehyde-3-phosphate dehydrogenase; H&E, Hematoxylin and eosin; HFD, high-fat diet; HG, high glucose; Icam1, Intercellular Adhesion Molecule 1; IL1β, interleukin 1 beta; IL6, interleukin 6; LFD, low-fat diet; LPS, lipopolysaccharide; MD2, Myeloid differentiation 2; MTT, methyl thiazolyl tetrazolium; MyD88, myeloid differentiation factor 88; NF-κB, Nuclear factor kappa-B; OCT, Optimal Cutting Temperature compound; PA, palmitic acid; PAS, periodic acid schiff; qPCR, quantitative Polymerase Chain Reaction; RASIs, renin-angiotensin system inhibitors; SDS-PAGE, sodium dodecyl sulfate polyacrylamide gel electrophoresis; T1DM, type 1 diabetes mellitus; T2DM, type 1 diabetes mellitus.; TGFB1, transforming growth factor beta 1; TLRs, Toll-like receptors; TNF-α, tumor necrosis factor-α. Vcam1, vascular cell adhesion molecule 1.

* Corresponding author at: Department of Cardiology, the First Affiliated Hospital of Wenzhou Medical University, Wenzhou, Zhejiang 325035, China.
E-mail address: wzmcliangguang@163.com (G. Liang).

https://doi.org/10.1016/j.biopha.2023.115660
Received 26 July 2023; Received in revised form 2 October 2023; Accepted 4 October 2023
Available online 7 October 2023

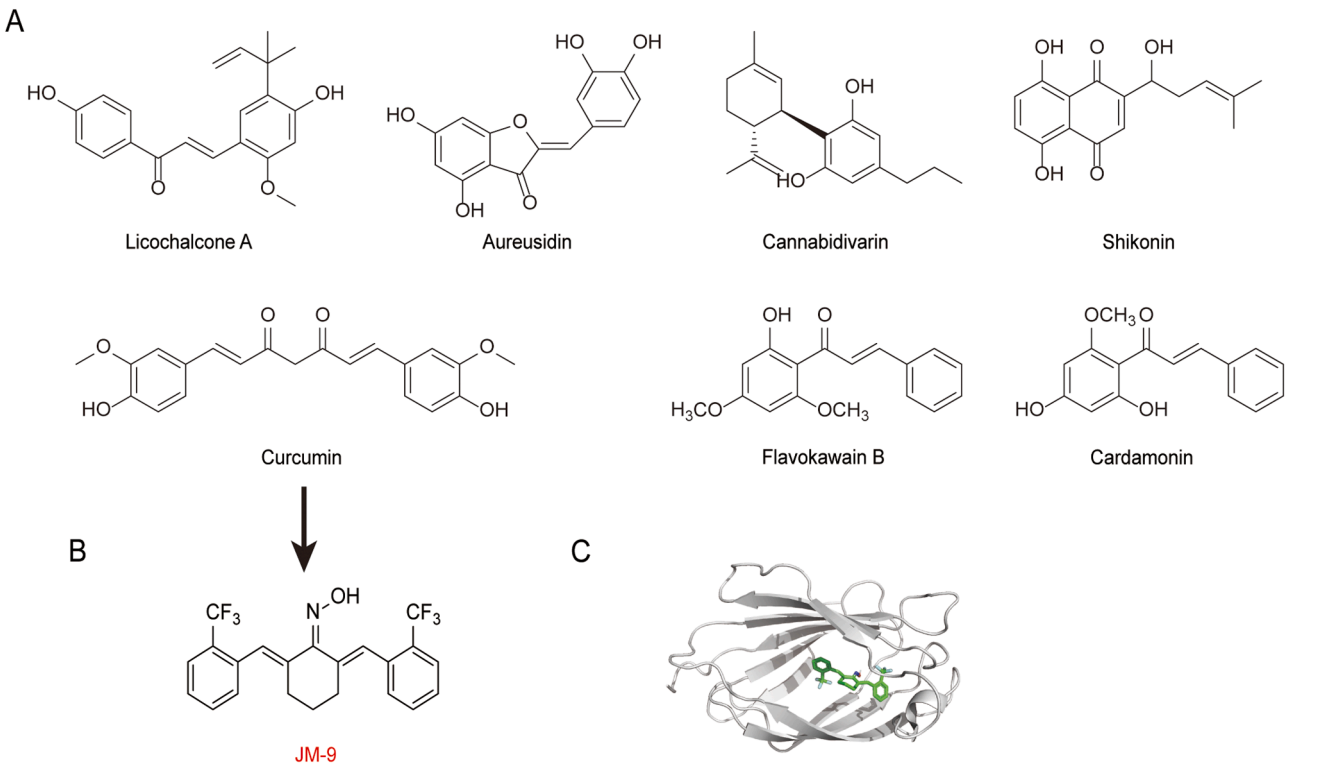

Fig. 1. JM-9 is a new MD2 inhibitor. (A) The chemical structures of MD2 inhibitors. (B) The chemical structures of JM-9. (C) Molecular docking results displaying the binding of JM-9 to rMD2 (PDB: 2E56) as determined by the Tripos molecular modeling software.

pathological process in DKD [5]. In all stages of DKD, immune cells, mainly macrophages, infiltrating the glomeruli and interstitium are a common occurrence [6]. Toll like receptors (TLRs) critically impact the innate immunity. The putative role of TLRs, particularly TLR2 and TLR4, in orchestrating intrarenal inflammation in DKD has been reported [5, 7–9]. Inhibition of the TLR signaling may confer renal protection in diabetic animals. Under hyperglycemia or high-concentration glucose (HG) conditions, due to the TLR4 activation, intracellular myeloid differentiation factor 88 (MyD88) is recruited and the pro-inflammatory signaling cascades (MAPKs and NF-κB) are subsequently activated [10]. That leads to secretion of inflammatory cytokines to induce renal inflammation and injuries [11].

As a indispensable co-receptor of TLR4, myeloid differentiation 2 (MD2) effectively assists in the LPS recognition by TLR4 [12]. In our previous report, MD2 is needed for HG-induced TLR4 activation. HG directly induces MD2/TLR4 complex formation for the TLR4-MyD88-MAPKs/NF-κB proinflammatory cascade activation [13]. DKD development was inhibited in the MD2$^{-/-}$ mice [14]. An MD2 inhibitor, L6H9, was found to attenuate renal inflammation, fibrosis, and dysfunction in T1DM mice by inhibiting the MD2-TLR4/MyD88 signaling pathwa y [14]. These previous findings indicate that MD2 is the predominant mediator of renal inflammation in DKD.

Natural products exert a crucial influence in the exploration of novel pharmaceuticals. Recently, several natural products with anti-inflammatory activity have been identified as small-molecule MD2 inhibitors, including Licochalcone A [15], Aureusidin [16], Cannabidivarin [17], Shikonin [18], Curcumin [19], Flavokawain B [20] and Cardamonin [21](Fig. 1A). Our group is engaging in discovering new and excellent MD2 inhibitor from the natural anti-inflammatory compounds. Based on the structure of curcumin, a natural MD2 inhibitor, we recently designed and synthesized a new small-molecule MD2 inhibitor with a stable chemical, JM-9 (Fig. 1B), which shows anti-inflammatory function in vitro. Molecular docking software revealed the potential binding between JM-9 and MD2 protein (Fig. 1C). Therefore, we hypothesized that JM-9 alleviates DKD by targeting MD2 and inhibiting renal inflammation. Presently, we observed that JM-9 inhibited both inflammatory and fibrotic responses in mouse primary peritoneal macrophages (MPMs) and renal epithelial cells, respectively. Orally administered JM-9 significantly suppressed diabetic mice' renal inflammation and fibrosis. Hence, JM-9 is a potential candidate for DKD treatment.

2. Methods

Supplementary Table S1 describes detailed reagent information. Supplementary Table S2 gives the primer sequences used in real-time qPCR assay.

2.1. Cell cultures

NRK-52E cell line (cat# GNR 8), a rat tubular epithelial cell (TEC) line, was provided by the Shanghai Institute of Biochemistry and Cell Biology. The cells were under the culture of DMEM with 10% FBS, 1% penicillin/streptomycin at 37C in a humidified incubator containing 5% CO_2.

The preparation of MPMs from male C57BL/6 mice and MD2 knockout (MD2$^{-/-}$) mice followed previous description. In brief, mice were stimulated by intraperitoneally injected with 6% thioglycolate solution (0.3 g beef extract, 0.5 g sodium chloride and 1 g tryptone in 100 ml ddH2O, a 0.22 μm filter was used for filtering; 2 ml/mouse) and placed in an environment free of pathogen for three days to receive cell isolation. 8 ml RPMI-1640 medium were employed to wash the peritoneal cavity, for harvesting total MPMs. After centrifugation, the cell collection medium was resuspended in RPMI-1640 medium with 1% penicillin/streptomycin and 10% FBS. After preparation at 700,000 cells/35 mm diameter well, primary cultures were plated first and used 4 h later. At 4 h after cell seeding, we removed non-adherent cells through medium washing.

2.2. Synthesis and structural identification of JM-9

Compound JM-9 synthesis was conducted in our laboratory. A solution of (2E,6E)− 2,6-bis(2-(trifluoromethyl)benzylidene)cyclohexanone (1 mmol) in EtOH (5 ml) was added the mixture of hydroxylamine hydrochloride (1 mmol) and pyridine (2 mmol). This reaction mixture was stirred at 80 ℃ for 4 h. And then, water was added to the mixture and extracted with ethyl acetate three times. The organic layer was dried with MgSO4, filtered and concentrated under vacuum. The obtained residue was purified by column chromatography to afford JM-9. The ^{1}H NMR and ^{13}C-HMR spectra data of JM-9 were recorded on a 400 MHz spectrometer (Bruker Corporation, Switzerland) with TMS as an internal reference, and the chemical shifts were reported in parts per million (Fig. S1A-B). ^{1}H NMR (400 MHz, $CDCl_3$) δ ppm 7.66 (t, $J = 8.5$ Hz, 2 H), 7.54–7.46 (m, 2 H), 7.44 (t, $J = 7.6$ Hz, 1 H), 7.41–7.32 (m, 3 H), 7.29 (dd, $J = 14.9$, 7.5 Hz, 2 H), 2.49–2.33 (m, 4 H), 1.63–1.52 (m, 2 H). ^{13}C NMR (100 MHz, $CDCl_3$) δ ppm 156.57, 138.47 (2 C), 135.81, 135.66, 132.31 (2 C), 131.29 (2 C), 131.20, 131.03, 130.50 (2 C), 127.21, 127.16, 125.85–125.74 (2 C), 123.97 (2 C), 29.20, 28.86, 25.07. A high-performance liquid chromatography method using Agilent 1260 HPLC System fitted with an Inertex C18 column (150 mm × 4.6 mm, 5 μM particle size) was used to ascertain the purity of compound JM-9 is 97.6% (Fig. S1C). In in vitro or in vivo studies, JM-9 was used after dissolving it in 1% sodium carboxyl methyl cellulose or dimethyl sulfoxide (DMSO), respectively.

2.3. Animal experiments

The Animal Policy and Welfare Committee of Wenzhou Medical University approved the employment of animals in this study (Approval Document No. wydw2020–0117). All animal experiments were carried out as per the NIH guidelines.

Male C57BL/6 J mice (weight 18–22 g) were obtained from the Wenzhou Medical University Animal Center. Eleven-week-old male db/m control mice and db/db mice came from GemPharmatech (Nanjing, China). Diabetic models extensively adopt male mice. Male MD2$^{-/-}$ mice (B6.129P2-Ly96 KO) with a C57BL/6 background were purchased from the Riken BioResource Center (Tsukuba, Ibaraki, Japan). We cultured the mice in a room free of pathogen with a 12:12 h light–dark cycle, and fed them with routine water and diet for rodents. The mice were randomly devided into different treatment groups.

Establishment of T1DM: 12 male C57BL/6 mice (7 weeks old) were intraperitoneally administered with 50 mg/kg streptozotocin (STZ; in a pH = 4.5 0.1 mol/L sodium citrate buffer,) for consecutive five days. Mice in the control group (n = 6, 7 weeks old) received identical volume of citrate buffer. A glucometer was employed to measure the blood glucose (BG) level on day 7. Mice of which the FBG levels > 16.6 mM were regarded diabetic. We provided mice with water and normal diet for rodent. On the 9th week following diabetes onset, we randomized 12 diabetic animals into T1DM (n = 6) group, and JM-9 (10 mg/kg/day)-treated T1DM (n = 6) group. The JM-9-treated group was orally administered with JM-9 (10 mg/kg/day) for eight weeks (from 9th to 16th week), with 1% CMC-Na solution being JM-9 administration vehicle. The T1DM group and control group (matched in age, n = 6) received 1% CMC-Na solution separately, as per the same schedule. Our team members recorded body weight (BW) and BG levels twice a week.

T2DM models were developed as previously described[22]: Based on fasting blood glucose (FBG) levels, 18 male C57BL/6 mice fell into 3 groups (n = 6): low-fat diet group (LFD), high-fat diet group (HFD), and JM-9-administered HFD group (at 20 mg/kg twice a day). The LFD involves 20 kcal.% protein, 10 kcal.% fat, and 70 kcal.% carbohydrate. The HFD involves 20 kcal.% protein, 60 kcal.% fat, and 20 kcal.% carbohydrates (cat. #MD12033). We fed mice for twenty four weeks. JM-9-treated groups were orally administered with JM-9 (20 mg/kg) each two days for eight weeks (from 16th to 24th week), comparatively, the HFD and LFD groups were treated with identical volume of vehicle (1% CMC-Na solution). Our team members recorded BW weekly, and BG levels twice a week.

db/db type 2 diabetic models: male *db/db* mice (11 weeks old) and *db/m* control mice (11 weeks old) were randomized into 4 groups according to FBG levels: *db/m* control group (*db/m*, n = 6), *db/db* model control group (n = 6), 25 mg/kg/day irbesartan-administered db/db mice (n = 6), and 25 mg/kg/day JM-9-administered T2D mice (n = 6). Irbesartan- or JM-9-treated groups were orally administered with irbesartan (25 mg/kg/day) or JM-9 (25 mg/kg/day) each two days for eight weeks. All mice received water and standard rodent diet. BWs were measured twice a week after starting administration, FBG levels were measured once at week 0, 4, 6 and 8, while urine was collected after 24 h.

We sacrificed mice after treatment to collect blood and renal tissue. Kidney functions were assessed by measuring serum creatinine, urinary albumin, and urinary creatinine levels. Urinary microalbumin and creatinine levels were detected and used to calculate the urine albumin/creatinine ratio (UACR). Glycocated hemoglobin, blood biochemistry (creatinine and urea nitrogen) and serum creatinine clearance rates were calculated at the end of the trial. Kidney tissues received fast freezing treatment in liquid nitrogen. The gene and protein expression in kidney tissues were analyzed. After being fixed in 4% paraformaldehyde, tissues underwent histological analyses via staining.

2.4. Kidney tissue staining

The kidney tissues underwent fixation treatment in 4% paraformaldehyde, followed by being paraffin embedded. Then they were cut into 5-μm thick sections. These dehydrated sections received H&E staining for histopathological analysis under the assistance of a light microscope. Masson's Trichrome and Sirius Red Staining also assists in assessing renal fibrosis while PAS staining was performed for renal collagen deposition assessment.

Specific to immunohistochemistry, sections underwent deparaffinization, hydration, and antigen retrieval under heating (pH = 6.0, 0.01 M sodium citrate buffer). The slides received half an hour of blocking in 3% hydrogen peroxide and half an hour of blocking in 1% BSA. They were subjected to one night of incubation in F4/80 antibodies (1:200) at 4 °C. The next day, they underwent one hour of incubation in secondary antibodies labeled by horseradish peroxidase (HRP) at 37 °C. Diaminobenzidine (DAB) staining served for the immunoreactivity detection. The slides received hematoxylin counterstaining. Imaging was performed by bright field microscopy (Nikon TE2000). Image J software, version 1.53i (NIH; Bethesda) served for quantitating the positively stained cells.

2.5. Western blot and immunoprecipitation

Protein isolation was carried out using the RIPA lysis and extraction buffer, while the concentration of the isolated proteins was determined using the Pierce BCA Protein Assay Kit. Protein lysates were separated through sodium dodecyl sulfate-polyacrylamide gel electrophoresis, followed by their transfer onto polyvinylidene fluoride membranes. The membranes were then subjected to a one-hour blocking step in Tris-buffered saline (pH 7.4), containing 0.05% Tween 20% and 5% non-fat milk, at room temperature. Subsequently, the membranes were incubated overnight with primary antibodies at 4 ℃, followed by a one-hour incubation with secondary antibodies at 25 ℃. Immunoreactivity was visualized using an enhanced chemiluminescence reagent (Bio-Rad Co. LTD), and the quantification was performed using Image J analysis software version 1.53i. The values were then subjected to normalization.

Co-immunoprecipitation together with immunoblotting assessed the binding among proteins. We extracted cell and tissue total proteins with a cell lysis buffer for IP that contained a protease inhibitor cocktail. Protein lysates (500 μg) underwent one night of incubation in the presence of an anti-TLR4 antibody at 4 ℃, and then received two hours

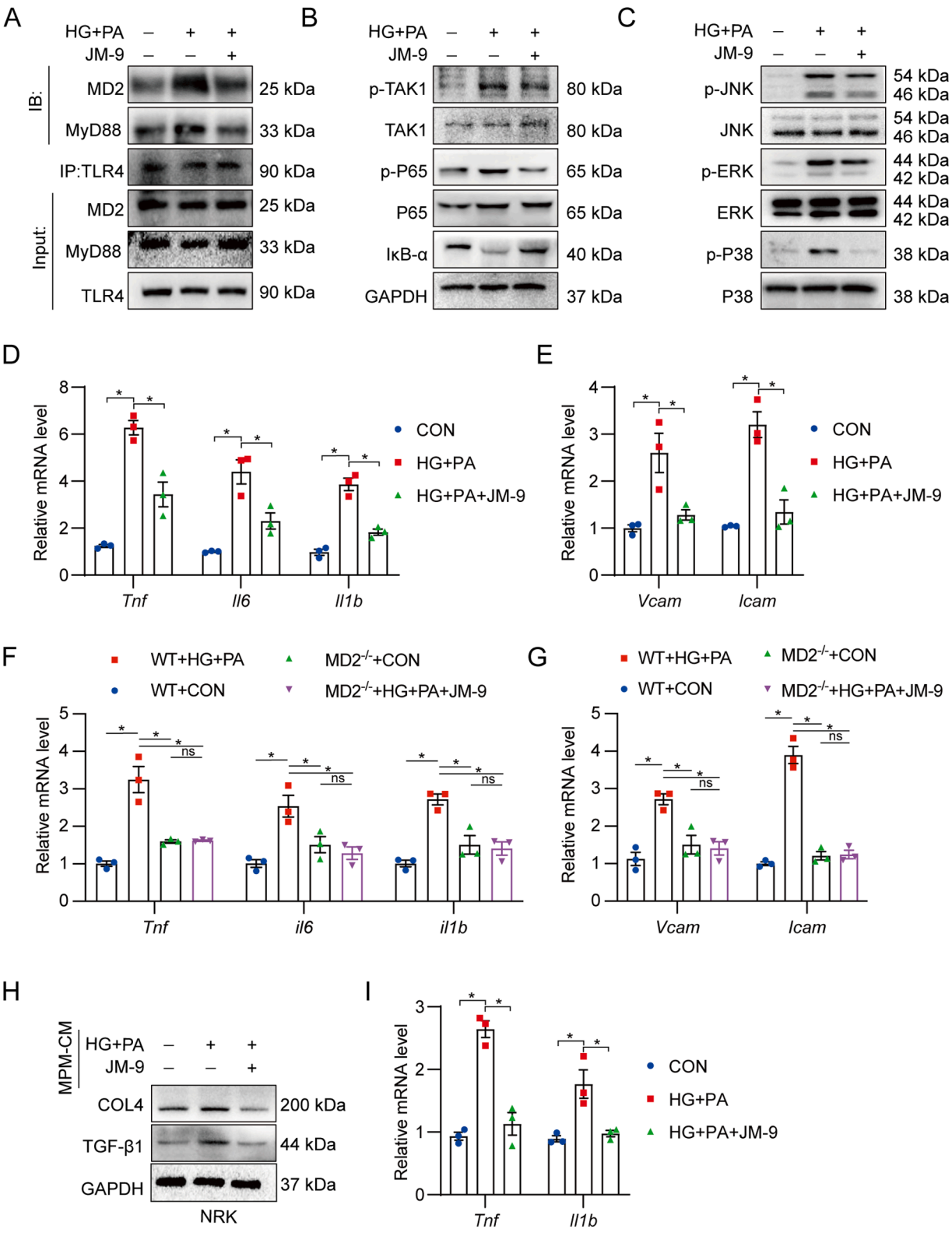

(caption on next page)

Fig. 2. JM-9 inhibit MD2-TLR4 pathway and inflammatory response in macrophages induced by HG+PA. (A) MPMs were pretreated with JM-9 (20 μM) for 1 h and then incubated with PA (200 μM) +HG (33 mM) for 30 min. The interactions among TLR4 (IP), MD2 (IB) and MyD88 (IB) were assessed by co-immunoprecipitation assay. (B) MPMs were pretreated with JM-9 (20 μM) for 1 h and then incubated with PA (200 μM) +HG (33 mM) for 1 h. Immunoblot analysis was performed to quantify the expression of NF-κB p65, TAK1 and IκBα in MPMs. Phosphorylated proteins and total proteins were measured. The GAPDH protein served as the internal reference. (n = 3; Mean ± SEM; *P < 0.05). (C) Immunoblot was performed to quantify the expression of JNK, ERK and P38 in MPMs. Phosphorylated proteins and total proteins were measured. GAPDH served as the internal reference protein. (n = 3; Mean ± SEM; *p < 0.05). (D) The mRNA levels of inflammatory genes (*Il6, Tnfa, and Il1b*) in MPMs. Data was normalized to *Actb* (n = 3; Mean ± SEM; *p < 0.05). (E) The mRNA levels of *Vcam1* and *Icam1* in MPMs. Data was normalized to *Actb* (n = 3; Mean ± SEM; *p < 0.05). (F-G) MPMs from WT and MD2$^{-/-}$ mice were pretreated with JM-9 (20 μM) for 1 h and then incubated with PA (200 μM) +HG (33 mM) for 12 h. The mRNA levels of genes (*Il6, Tnfa, Il1b*, *Vcam1,* and *Icam1*) in MPMs. Data was normalized to *Actb* (n = 3; Mean ± SEM; *p < 0.05). (H) MPMs were pretreated with JM-9 (20 μM) for 1 h and then exposed to HG and PA for 24 h. The cell culture supernatant (CM) was collected. NRK cells were exposed to MPMs CM for 24 h, and the protein levels of fibrotic proteins COL4 and TGF-β1 were detected. GAPDH served as the internal reference protein. (I) NRK cells were incubated with MPMs CM for 24 h, and the mRNA levels of inflammatory cytokines in MPMs were detected by RT-qPCR. Data was normalized to *Actb*. (n = 3; Mean ± SEM; *P < 0.05).

of shaking immunoprecipitation in protein A/G agarose beads at RT. Bead-protein complexes underwent centrifugation treatment for collection, and were washed thrice using PBS. At last, the complex was heated to be dissociated and Western blotting and immunoblotting antibody served for analyzing the target MyD88 or MD2 proteins regarding TLR4.

2.6. Real-time qPCR

mRNA expression level analysis was conducted using real-time qPCR. Total RNA from kidney tissues, MPMs, or NRK-52E cells was extracted using Trizol Reagent. The extracted RNA was then reversely transcribed into cDNA using the PrimeScript RT reagent. For real-time PCR, the TB Green Premix Ex Taq II was employed on a CFX96 Touch Real-Time PCR Detection System (Bio-Rad). The gene primers used here were synthesized by Invitrogen (Supplementary Table S1).

2.7. JM-9-to-MD2 molecular docking

AutoDock (a version 4.2.6, from Scripps Research, La Jolla) served for the molecular docking simulation. The crystal structure exhibited by the human MD2 lipid IVa complex with the PDB code 2E59 came from the Protein Data Bank. AutoDock Tools (version 1.5.6) was used to generate the docking input files and then analyze the docking results.

2.8. Cell viability assay

The viability of MPMs was measured by cell counting Kit8 (CCK-8) assay. MPMs were seeded into 96-well plates at a density of 5000 cells per well. Subsequently, MPMs treated with JM-9 at different concentrations at 37 ℃ for 24 h. Post a 24-hour incubation period, 10 μL of CCK-8 solution (Solarbio Life Science, Beijing, China) was administered to each well, and the cells were further incubated for an additional 4 h. The resulting cell viability or proliferation was determined by assessing the OD450 using a SpectraMax® M5 Multi-Mode Microplate Reader.

2.9. Statistical analysis

All assays were randomized and blinding method was adopted. Data are in the form of mean ± SEM. The GraphPad Prism 8.0 software assisted in the statistical analyses. The one-way ANOVA together with Dunnett's post hoc test served for the mean value comparison between two groups while one-way ANOVA, nonparametric Kruskal–Wallis test, together with Dunnett's post hoc test served for the mean value comparison among multiple independent groups. $p < 0.05$ reported statistical significance. Post-test was conducted only when F achieved $p < 0.05$ and homogeneity did not change remarkably.

3. Results

3.1. JM-9 inhibited MD2-TLR4 pathway and inflammation in HG+PA-induced macrophages

First, we determined whether JM-9 can affect the assembly of MD2/TLR4/Myd88 interaction in MPMs. The CCK8 assay showed that JM-9, at concentrations ranging from 0.05 to 40 μM, did not show significant toxicity in MPMs (Fig. S2A). Thus, we used JM-9 at 20 μM in the in vitro study. As found, HG and palmitic acid (PA) significantly activated the MD2-TLR4 signaling pathway (Fig. 2A, Fig. S2B). Pretreatment with JM-9 (20 μM), which inhibited the MD2-to-TLR4 binding, suppressed MyD88 recruitment to TLR4. Pretreatment of MPMs with JM-9 also inhibited TAK1 phosphorylation and activation regarding NF-KB and MAPKs pathways (Fig. 2B-2 C, Fig. S2C-S2D). The activation of the innate immune response, along with persistent low-level inflammation show a clear relevance to diabetes pathogenesis as well as its microvascular complications. The onset and progression of DKD are influenced by the function of inflammatory cytokines. Pretreatment with JM-9 inhibited the HG- and PA-induced expressions regarding adhesion molecules and inflammatory cytokines (Fig. 2D-2E). We also examined whether JM-9 inhibited inflammation by relying on targeting MD2 in MPMs. MPMs isolated from C57BL/6 wildtype and MD2$^{-/-}$ mice respectively were pretreated with 20 μM JM-9 for 1 h and then exposed to PA+HG for 12 h. Our results showed that JM-9 failed to further reduce the mRNA levels of inflammatory cytokines and adhesion molecules in HG+PA-challenged MPMs when MD2 was deleted (updated Fig. 2F-G), indicating that JM-9 suppressed inflammatory factor expressions in macrophages through targeting MD2. Macrophage-secreted inflammatory cytokines can exacerbate the inflammatory responses, fibrosis, and necroptosis of intrinsic renal cells[23]. Therefore, we investigated whether the macrophage-derived inflammatory cytokines could result in pathological changes in NRK cells. MPMs were pre-treated with JM-9 for a duration of 1 h, after which they were exposed to HG and PA for a period of 12–24 h, followed by collecting the condition media (CM) of cells. Then, the collected CM was exposed to NRK cells. Pretreatment with JM-9 significantly alleviated fibrosis and inflammation in NRK cells (Fig. 2H-I). These findings indicate that JM-9 suppressed inflammatory factor expressions in macrophages through suppressing the MD2-TLR4 signaling pathway, which leads to renal cell fibrosis and inflammation.

3.2. JM-9 prevented STZ-induced renal dysfunction and fibrosis in T1DM mouse model

Given that JM-9 could alleviate HG- and PA-induced inflammatory damage and fibrosis in renal cells in vitro, we validated the efficacy of JM-9 in DKD mice. We used STZ for inducing T1DM in male C57BL/6 mice (7 weeks old), using JM-9 (10 mg/kg/day) to treat the mice by gavage from week^{9} to week^{16}. We selected the dose of JM-9 according to our previous study in which the pharmacological effects of another small-molecule MD2 inhibitor at 10 mg/kg/day was investigated in

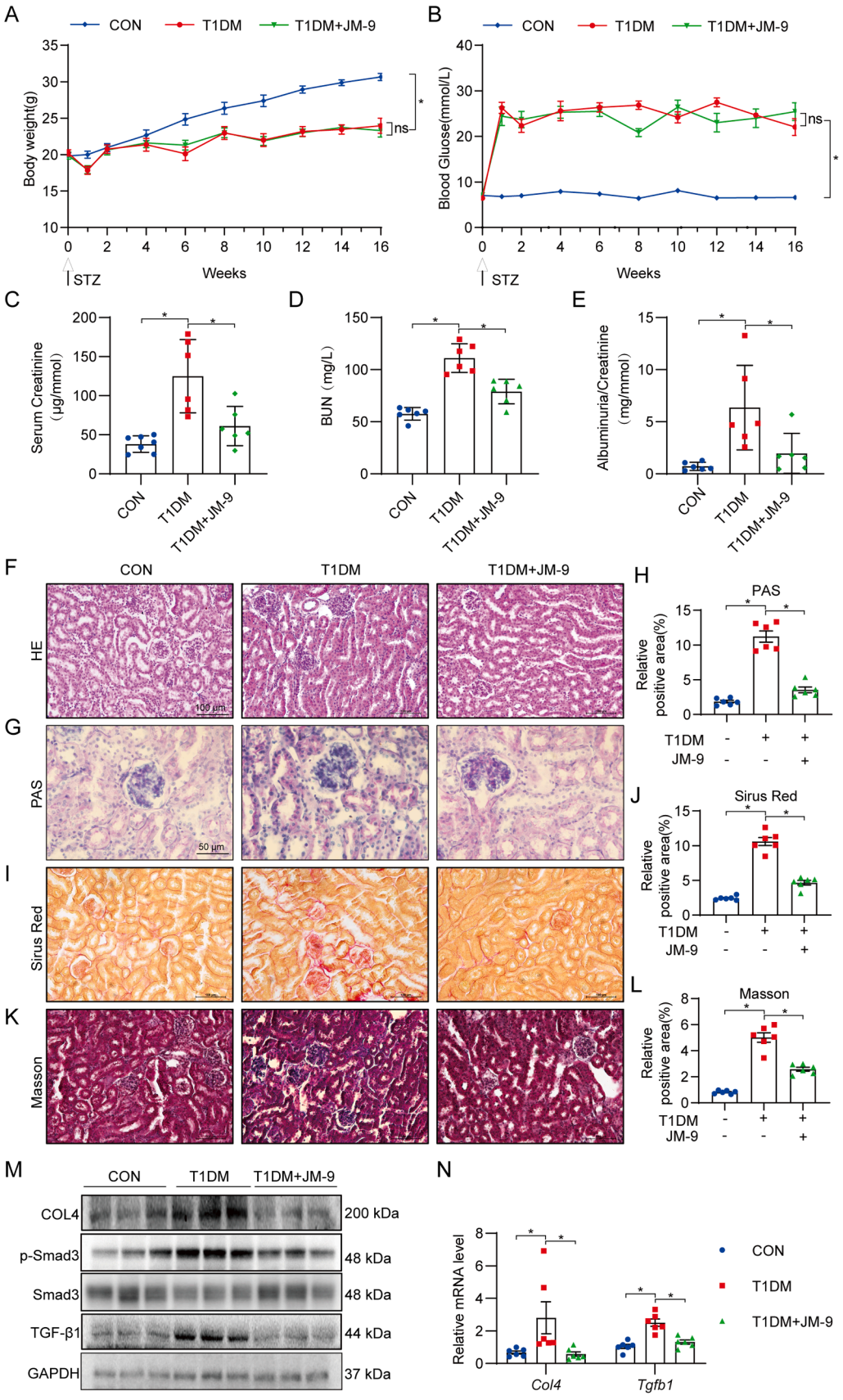

(caption on next page)

Fig. 3. JM-9 prevents renal functional and structural deficits in STZ-induced T1DM mice. The animal trials were executed following the techniques mentioned in the "Methods" segment. (A) Body weights were recorded weekly (n = 6; Mean ± SEM; *P < 0.05). (B) Blood glucose levels in mice were recorded twice a week. (n = 6; Mean ± SEM; *P < 0.05). The corresponding commercial kits were employed for detecting the levels of serum creatine (C), blood urea nitrogen (D), and urine albumin to creatinine ratio (E). (F) Hematoxylin and eosin (H&E) staining of renal tissues. [scale bar = 100 μm]. (G-H) PAS-stained images of renal tissues. [scale bar = 50 μm] (n = 6; Mean ± SEM; *P < 0.05). (I-J) Fibrosis in renal tissues was determined by Picro Sirius Red staining. [scale bar = 100 μm] (n = 6; Mean ± SEM; *P < 0.05). (K-L) Fibrosis in renal tissues was determined by Masson's Trichrome staining. [scale bar = 100 μm] (n = 6; Mean ± SEM; *P < 0.05). (M) Measurement of fibrosis-related proteins (COL4, p-Smad3/Smad3, and TGF-β1) in renal tissues. GAPDH served as the internal reference protein. (N) The mRNA levels of fibrosis-associated genes (*Col4,* and *Tgfb1)* in the renal tissues. Data was normalized to *Actb* (n = 6; Mean ± SEM; *P < 0.05).

mouse model of DKD [14]. The diabetic mice showed weight loss and increased BG levels, which were not affected by JM-9 treatment (Fig. 3A, B). The potential renoprotective activities of JM-9 were assessed by analyzing the renal functions. T1DM mice presented obviously elevated serum creatinine (Cr), UACR, and blood urea nitrogen (BUN), while such elevation was suppressed by JM-9 treatment (Fig. 3C-E). Therefore, JM-9 protected against renal dysfunctions in T1DM mice.

According to H&E staining kidney tissues, variation in structure and hypertrophy (abnormal glomeruli, manifested as mesangial proliferation and glomerular cluster disorders) could be observed in T1DM mice, relative to JM-9-treated mice (Fig. 3F). PAS staining showed that JM-9 alleviated glycogen deposition in T1DM (Figs. 3G, 3H). Our results have shown that JM-9 can significantly reduce the accumulation of collagen and fibrosis in T1DM kidney tissues (Fig. 3I-L). Protein and mRNA expressions regarding fibrosis-associated factors, Collagen type IV (Col-4) and TGF-β revealed that JM-9 exerted a protective effect in T1DM mouse kidneys; we also showed that JM-9 significantly inhibited Smad3 phosphorylation in T1DM mice (Fig. 3M-N, Fig. S3). Thus, JM-9 possibly assisted in preserving the kidney functions in T1DM mice as well as preventing matrix expansion.

3.3. JM-9 alleviated renal inflammation and macrophage infiltration in T1DM mice

In vitro, JM-9 inhibited the MD2-TLR4 pathway, suppressing macrophage-induced inflammation and NRK cell fibrosis as well as inflammation. Kidney tissue lysates underwent immunoprecipitation assay, accordingly, JM-9 remarkably suppressed MD2-TLR4-MyD88 interactions in T1DM mice (Fig. 4A, Fig. S4A). In tandem with JM-9-induced suppression of MD2, we observed increased IκBα levels and decreased p-TAK1, p-jnk, p-erk, p-p38, and p-p65 levels, indicating dampened NF-κB and MAPKs activities (Fig. 4B-4D, Fig. S4B). RT-qPCR showed that JM-9 significantly inhibited the expressions of STZ-induced renal inflammatory factors (*Il6, Il1b,* and *Tnfα*) (Fig. 4E-G). According to immunohistochemical staining, the F4/80 immunoreactivity exhibited by T1DM mice' renal tissues presented an obvious enhancement (Fig. 4H, Fig. S4C). Comparatively, treatment with JM-9 eliminated the macrophage infiltration increase to the largest extent. Hence, JM-9 protects kidneys from T1DM-induced damage by inhibiting MD2-mediated inflammation.

3.4. JM-9 alleviated renal dysfunctions and fibrosis in T2DM mice

For assessing how JM-2 affected T2DM, the same studies were conducted in mice suffering T2DM. As hypothesized, JM-9 may exert similar therapeutic effects in T2DM. Male C57BL/6 mice were fed with a high-fat diet for a period of 24 weeks, together with the assessment renal functions. Treatment with JM-9 did not lead to significant alterations in the BWs or the BG levels in T2DM mice, in tandem with findings from T1DM mice (Fig. 5A, B). Treatment with JM-9 suppressed serum creatinine, BUN, and UCAR levels (Fig. 5C–5E). According to H&E analysis on harvested renal tissues, structure and hypertrophy of T2DM mice altered, while such alternation was not observed in JM-9 treated mice (Fig. 5F). PAS staining revealed that JM-9 alleviated glycogen deposition (Fig. 5G, H). JM-9 treatment remarkably enhanced the collagen deposition increase in the kidneys(Fig. 5I-L), which was confirmed by the examination on the protein levels of Col4, p-Smad3, and TGF-β (Fig. 5M-N, Fig. S5). Our findings suggest that JM-9 prevented renal fibrosis in T2DM mice. In summary, JM-9 protected against renal dysfunction and fibrosis in T2DM mice.

3.5. JM-9 alleviated renal inflammation and macrophage infiltration in T2DM mice via suppressing the MD2-TLR4 pathway

As was found in T1DM mice, the HFD-induced T2DM mice exhibited increased MD2-TLR4-MyD88 complex levels in kidney tissues, compared to the control group. Treatment with JM-9 inhibited MD2 activation in T2DM mice kidneys (Fig. 6A, Fig. S6A). Phosphorylated (p)-p65, p-TAK1, p-JNK, p-ERK, and p-P38 showed elevated levels while lysates from T2DM mice presented worse IκB levels, relative to JM-9–treated mice (Fig. 6B-6D, Fig. S6B). RT-qPCR showed that JM-9 significantly alleviated the expressions of inflammatory factors in T2DM mice (Fig. 6E-G). According to immunohistochemical staining, compared to kidney tissues from control mice, kidney tissues from obese mice presented obviously strengthened F4/80 immunoreactivity (Fig. 6H, Fig. S6C). Macrophage infiltrations were increased in HFD-induced T2DM renal tissues. JM-9 treatment alleviated the macrophage infiltration elevation to the largest extent. Taken together, JM-9 protects kidneys from HFD-induced T2DM by inhibiting MD2-mediated inflammation.

3.6. JM-9 alleviated renal dysfunction and renal fibrosis in the db/db mice

To confirm the renoprotective properties of JM-9, we paid further attention to *db/db* mice and used irbesartan as the positive control drug. Eleven-week old *db/db* diabetic mice received 8 weeks of treatment of 25 mg/kg of JM-9 or 25 mg/kg irbesartan. *db/db* group showed obviously higher BWs and FBG levels compared to *db/m* group. BWs and BG levels did not change largely after *db/db* mice were treated with JM-9 and irbesartan (Fig. 7A, B). Relative to the *db/db* group, levels of Cr, BUN, UCAR, and creatinine clearance rate in the irbesartan group and JM-9 group mice were significantly reduced (Fig. 7C-7 F). H&E staining showed that pathological changes, such as patchy necrosis, interstitial fibrous tissue proliferation and inflammatory cell infiltrations were observed in *db/db* mice' renal tissues. Treatment with JM-9 attenuated the pathological changes in *db/db* mice kidneys (Fig. 7G). According to PAS staining, JM-9 alleviated glycogen deposition in *db/db* renal tissues (Figs. 7H, I). According to sirius red staining (Fig. 7J, K) and Masson's trichrome staining (Fig. 7L, M), the groups treated with JM-9 and irbesartan showed a significant improvement in collagen deposition in the kidney tissues of db/db mice. In summary, JM-9 exerted protective effects on renal dysfunctions and renal fibrosis in the *db/db* diabetic mice.

4. Discussion

Building on the study regarding natural products with anti-inflammatory properties and target MD2, we discovered a novel and natural product-derived MD2 inhibitor (JM-9). Our study focused on the possible therapeutic effects exerted by the JM-9 in DKD. Exposure of cultured MPMs to HG and PA with JM-9 suppressed MD2 activities, the relation to TLR4, MAPK, and NF-κB signaling pathway activation and triggering of downstream inflammatory cytokines. These macrophage-

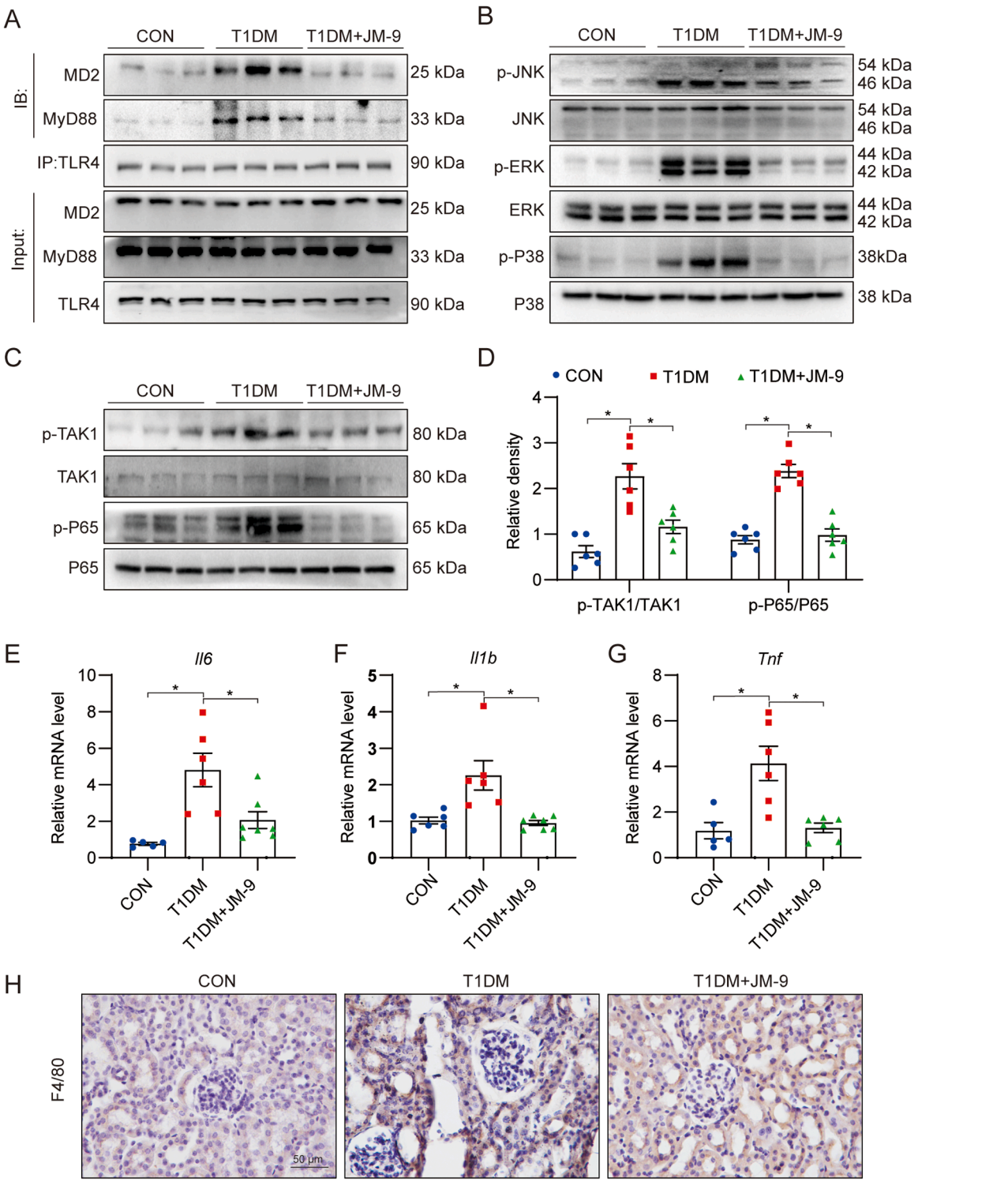

Fig. 4. JM-9 prevents MD2 activation and inflammatory responses in STZ-induced diabetic mice. (A) The coprecipitation analysis outcomes for the MD2-TLR4-MyD88 complex in T1DM kidney samples. TLR4 antibody was used to immunoprecipitate lysates, which were then scrutinized for MD2. The lower panel illustrates densitometric quantification of the results. (B) The expression of JNK, ERK, and P38 were analyzed via immunoblotting in renal tissues of T1DM mice. Phosphorylated proteins and overall proteins were assessed, while GAPDH was employed as the control protein. (n = 6; Mean ± SEM; *P < 0.05). (C-D) The expression of NF-κB p65, TAK1 and IκBα were analyzed via immunoblotting in renal tissues of T1DM mice. Phosphorylated proteins and overall proteins were assessed, while GAPDH was employed as the control protein. (n = 6; Mean ± SEM; *P < 0.05). (E-G) The mRNA levels of inflammatory genes (*Il6, Il1b* and *Tnfa)* in the renal tissues. Data was normalized to *Actb* (n = 6; Mean ± SEM; *P < 0.05). (H) Staining of T1DM renal tissues of mice for macrophage marker F4/80. Sections were counterstained with hematoxylin (blue). [scale bar = 50 μm].

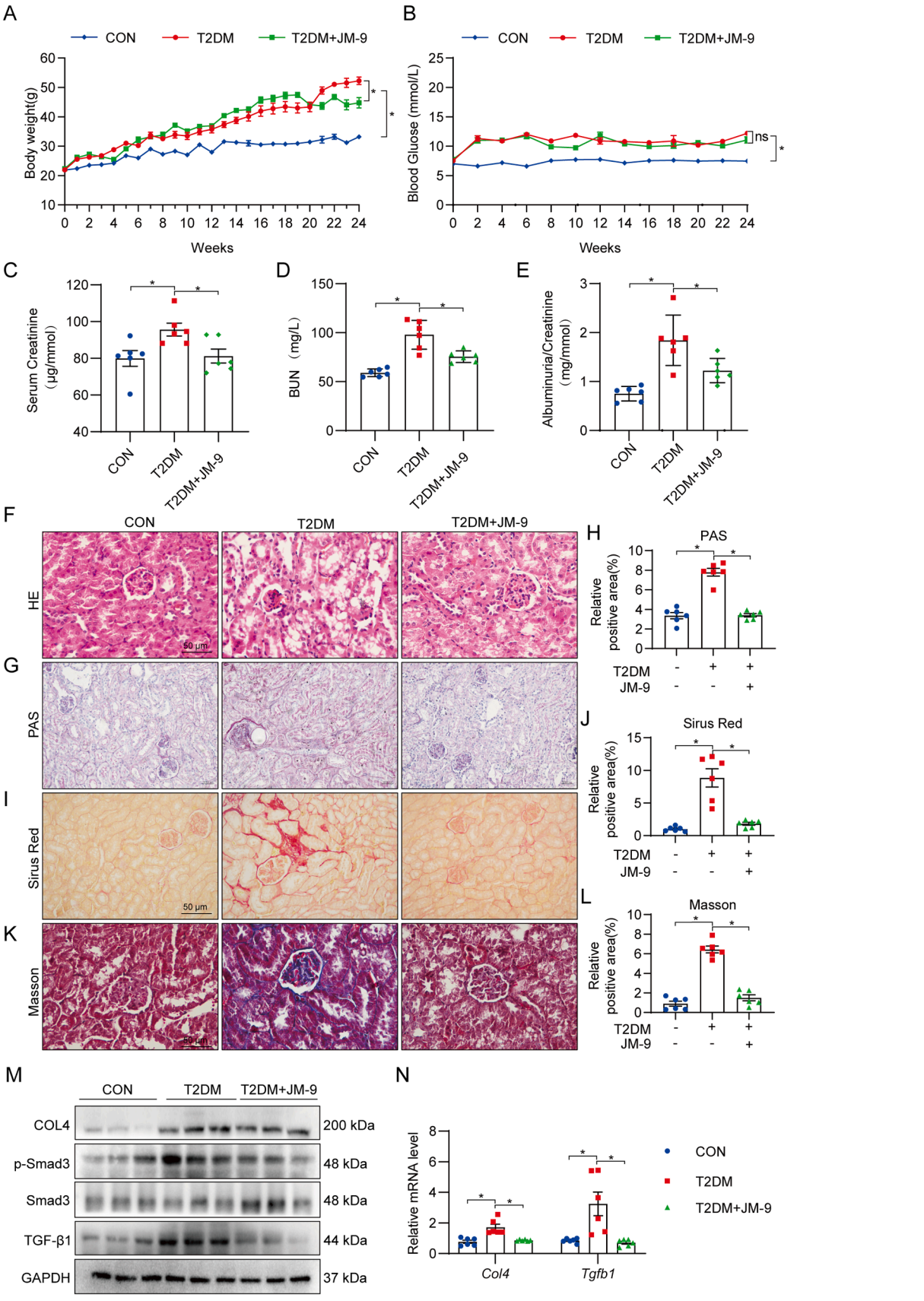

(caption on next page)

Fig. 5. JM-9 prevents renal functional and structural deficits in HFD-induced T2DM mice. The animal trials were executed following the techniques mentioned in the "Methods" segment. (A) Body weights were recorded weekly (n = 6; Mean ± SEM; *P < 0.05). (B) The corresponding commercial kits were employed for detecting the levels of serum creatine (C), blood urea nitrogen (D), and urine albumin to creatinine ratio (E). (F) Hematoxylin and eosin (H&E) staining of renal tissues. [scale bar = 100 μm]. (G-H) PAS-stained images of renal tissues. [scale bar = 50 μm] (n = 6; Mean ± SEM; *P < 0.05). (I-J) Fibrosis in renal tissues was determined by Picro Sirius Red staining. [scale bar = 100 μm] (n = 6; Mean ± SEM; *P < 0.05). (K-L) Fibrosis in renal tissues was determined by Masson's Trichrome staining. [scale bar = 100 μm] (n = 6; Mean ± SEM; *P < 0.05). (M) Measurement of fibrosis-related proteins (COL4, p-Smad3/Smad3, and TGF-β1) in renal tissues. GAPDH was used as control. (N) The mRNA levels of fibrosis-associated genes (*Col4,* and *Tgfb1)* in the renal tissues. Data was normalized to *Actb* (n = 6; Mean ± SEM; *P < 0.05).

derived factors increased the fibrotic and inflammatory responses in renal TEC. However, no above effects were observed in the case that macrophage-derived factors from JM-9 treated macrophages were assayed. *In vivo*, treatment with JM-9 prevented renal dysfunctions, extracellular matrix production, and expressions of inflammatory factors accompanied by reduced MD2-TLR4 interactions in both T1DM and T2DM mice.

DKD has complex pathogenesis mechanisms, and they involve various pathways. In traditional sense, DKD is a non-inflammatory glomerular disease resulted from haemodynamic and metabolic variation. According to studies, systemic and local renal inflammation crucially impact DKD occurrence and progression [24,25]. The macrophages take part in the occurrence and progression of DKD. Renal macrophage accumulation shows an obvious relevance to Cr, the accumulation of interstitial myofibroblast as well as scores of interstitial fibrosis [26]. In diabetic *db/db* mice, accumulated and activated macrophage induces glomerular and tubular injury, resulting in renal fibrosis and upregulation of macrophage chemokines in the kidneys [27]. We found that HG and PA increased MD2-TLR4 binding in macrophages, leading to increased inflammatory responses. The renal biopsy samples from individuals with DKD exhibit elevated expression levels of growth factors, inflammatory cytokines, adhesion molecules and chemokines (such as IL-6, TNF-α, CC-chemokine ligand 2 and intercellular adhesion molecule 1) [28]. We discovered that the culture medium (CM) derived from macrophages induced fibrosis and inflammation of renal tubular cells. Chronic renal non-resolving inflammation enhances the fibrotic responses occurring in the disease [29]. Renal inflammation and fibrosis develop complexly, with many interacting pathways resulting in chronic inflammatory infiltrates, including macrophages as well as other immune cells releasing pro-fibrotic factors and cytokines [30]. They create pro-fibrotic microenvironments after interacting with the intrinsic kidney cells [31]. Therefore, persistent inflammation induces pro-fibrotic cascades in the kidneys [32].

The TLR4 signaling pathway is important for HG-induced renal inflammation in innate immunity [33]. TLR4 levels in TECs within the kidneys of patients with T1DM and T2DM have been shown to be elevated [5,34]. $TLR4^{-/-}$ mice were found to be protected from inflammation, fibrosis, albuminuria, and renal dysfunction induced by STZ [7,8]. Thus, TLR4 signaling pathway inhibition has an underlying therapeutic implications in DKD. The MD2 forms a complex with TLR4 to effectively bind LPS with a strong affinity. We found that MD2 has been identified as a crucial contributor in chronic inflammatory diseases, including AngII-induced kidney fibrosis [35]. Previously, it was found that MD2 presented an obvious over-expression and activation in diabetic mice kidney tissues. Further, MD2 deficient STZ-induced T1DM mice exhibited a notable safeguard against renal fibrosis and inflammation [14]. Based on previous findings, targeting MD2 to inhibit TLR4 signaling is considered a potential anti-inflammation strategy in DKD. The MD2 inflammasome promotes inflammation in DKD. The MD2-TLR4 complex recruits MyD88 and other adaptor proteins, as a result, a myddosome complex is formed, different signaling molecules, including NF-κB, MAPKs, and interferon regulatory factor, are activated, and then various cytokines and chemokines are produced and released subsequently [36]. The NF-κB and MAPKs signaling pathways activate potent proinflammatory cytokines to secrete in DKD [37–40]. Therefore, JM-9 effectively inhibits the NF-κB/MAPKs signaling pathway activation, alleviating renal inflammation.

In T2DM *db/db* mice, we used irbesartan as the positive control drug. Irbesartan is an AT1 angiotensin II receptor antagonist that is renoprotective in individuals diagnosed with T2DM and evident nephropathy [41,42]. The activation of renin-angiotensin system (RAS) and lipid disorders primarily report the risk of progressive chronic kidney disease. RAS inhibition is important for DKD treatment [43]. Elevated levels of local Ang II in diabetic kidneys stimulates the expressions level of TGF-β and promotes fibrosis in the kidneys, thereby exacerbating DKD development [44]. Previously, we found that MD2/TLR4 innate immune signaling was correlated with RAS activation in diabetic kidneys. MD2/TLR4 signaling pathway inhibition markedly suppressed the expressions of ACE and AT1 receptors, as well as Ang II production induced by HG in vivo and in vitro. These effects contributed to amelioration of DKD [14]. Thus, MD2 is an essential target for regulating local RAS in DKD. We postulated that the MD2 inhibitor (JM-9) alleviates DKD by impeding the activation of the NF-κB/MAPKs signaling cascades and down-regulating local RAS in diabetic kidneys. We found that compared to irbesartan, JM-9 exerted more robust therapeutic effects in *db/db* mice. Thus, JM-9 potentially exerts its effects by inhibiting both inflammation and RAS, whereas irbesartan only acts by inhibiting RAS. Studies should be conducted to determine whether JM-9 affects the RAS in diabetic kidneys.

Some issues have not been well explained in the study and need to be clarified in future investigations. It has been reported that some previously reported inhibitors (shown in Fig. 1A) interacts directly with MD2 protein and inserts into the pocket of MD2 structure. Thus, we speculate that JM-9, as a structurally similar MD2 inhibitor, also interacts directly with MD2. Although our studies simulated the interaction between JM-9 and MD2, it is necessary to determine the physically direct interaction between JM-9 and MD2 protein, and it is interesting to explore how JM-9 binds to MD2 protein. This limitation deserves to be noted in the further inverstigations. In addition, understanding the biodistribution and pharmacokinetics of drugs are crucial when exploring their efficacy. However, the pharmacokinetics and tissue distribution of JM-9 is not well understood. We will perform the formal pharmacokinetics study and safety evaluation for the pre-clinical development of JM-9 in the future. Although we demonstrated that JM-9 alleviated DKD in three models, the advantages of JM-9 compared with other MD2 inhibitors have not been elucidated. According to in vitro and in vivo studies, MD2 also participates in the development of other inflammation-related diseases, including diabetic cardiomyopathy [13], obesity [45], Vascular remodeling [46], colon cancer [47], acute lung injury [15]. Therefore, we suggest that JM-9 also has large potential as a therapeutic agent for not only other diabetic complications, but also for MD2-mediated inflammatory diseases. This hypothesis need to be further investigated.

In conclusion, we comprehensively demonstrate that JM-9 prevent DKD through suppressing the renal inflammation and fibrosis via target MD2. Based on T1DM and T2DM mice models, JM-9 treatment completely mitigated HG-induced inflammatory responses in kidney tissues. Mechanistically, JM-9 inhibited MD2-TLR4 interaction and the downstream MAPKs and NF-κB signaling pathways, thereby resisting renal inflammation, fibrosis, and dysfunction. Collectively, these results reveal the therapeutic effects of JM-9 on DKD and indicate its potential application in the treatment and management of DKD.

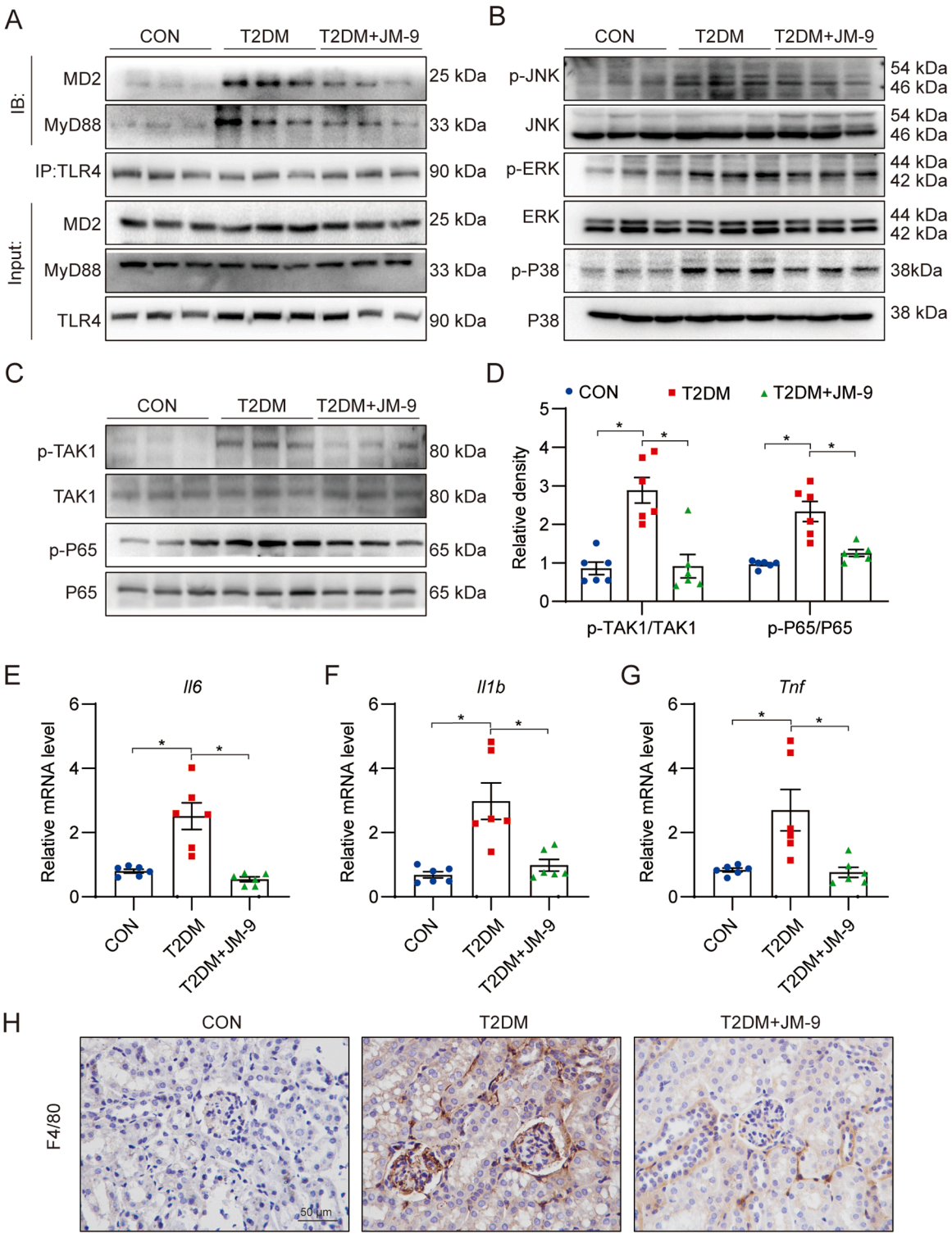

Fig. 6. JM-9 prevents MD2 activation and inflammatory responses in HFD-induced diabetic mice. (A) The coprecipitation analysis outcomes for the MD2-TLR4-MyD88 complex in T2DM kidney samples. TLR4 antibody was used to immunoprecipitate lysates, which were then scrutinized for MD2. The lower panel illustrates densitometric quantification of the results. (B) The expression of JNK, ERK, and P38 were analyzed via immunoblotting in renal tissues of T2DM mice. Phosphorylated proteins and overall proteins were assessed, while GAPDH was employed as the control protein. (n = 6; Mean ± SEM; *P < 0.05). (C-D) The expression of NF-κB p65, TAK1 and IκBα were analyzed via immunoblotting in renal tissues of T2DM mice. Phosphorylated proteins and overall proteins were assessed, while GAPDH was employed as the control protein. (n = 6; Mean ± SEM; *P < 0.05). (E-G) The mRNA levels of inflammatory genes (*Il6, Il1b* and *Tnfa)* in the renal tissues. Data was normalized to *Actb*. (n = 6; Mean ± SEM; *P < 0.05). (H) Staining of T1DM renal tissues from mice for macrophage marker F4/80. Sections were counterstained with hematoxylin (blue). [scale bar = 50 μm].

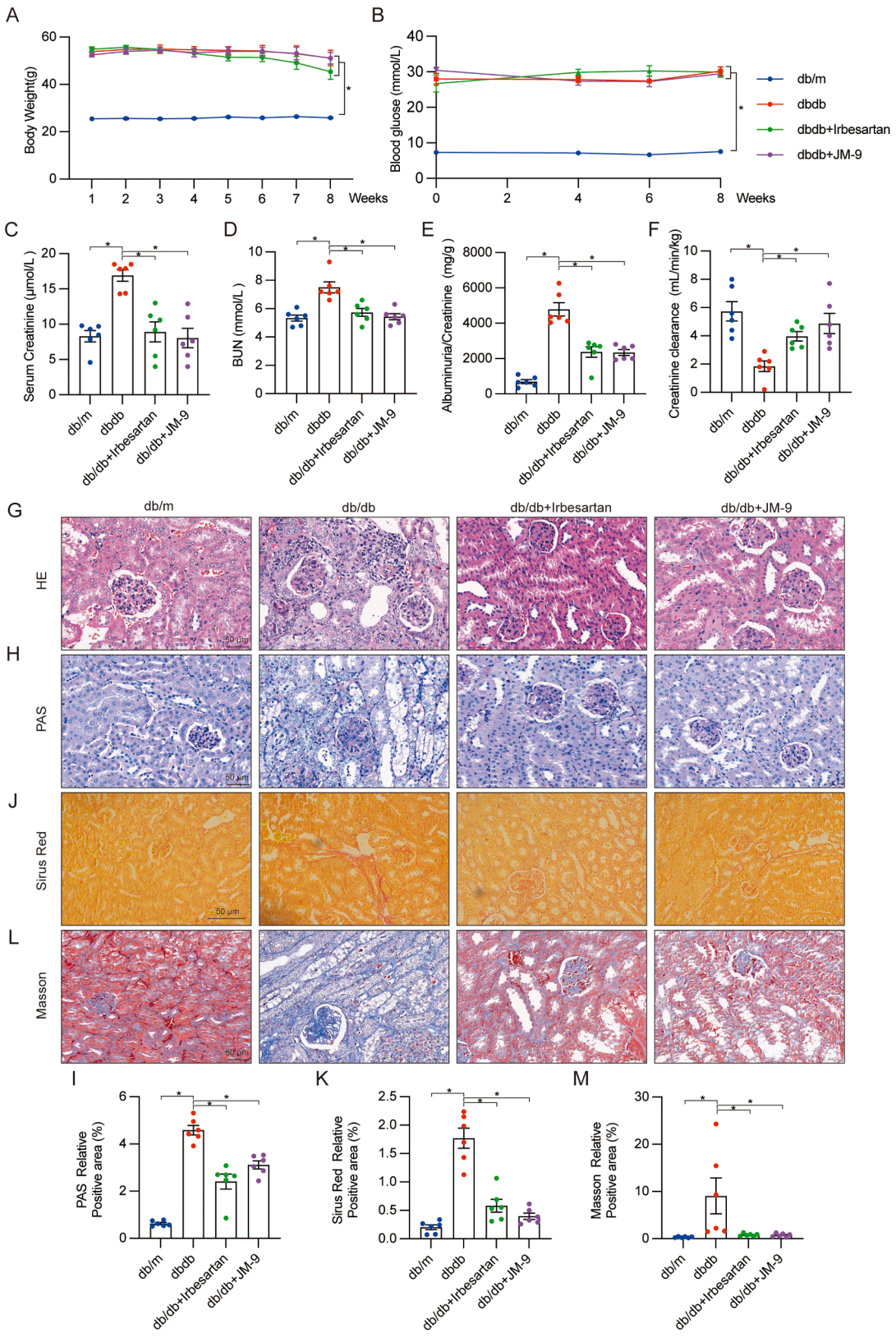

Fig. 7. JM-9 prevents renal functional and structural deficits in db/db mice. The animal trials were executed following the techniques mentioned in the "Methods" segment. (A) Body weights were recorded weekly. (n = 6; Mean ± SEM; *P < 0.05). (B) Blood glucose levels in mice were recorded twice a week. (n = 6; Mean ± SEM; *P < 0.05). Levels of serum creatine (C), blood urea nitrogen (D), urine albumin to creatinine ratio (E) and creatinine clearance (F) were examined using corresponding commercial kits. (G) Hematoxylin and eosin (H&E) staining of renal tissues. [scale bar = 50 μm]. (H-I) PAS-stained images of renal tissues. [scale bar = 50 μm] (n = 6; Mean ± SEM; *P < 0.05). (J-K) Fibrosis in renal tissues was determined by Picro Sirius Red staining. [scale bar = 50 μm] (n = 6; Mean ± SEM; *P < 0.05). (L-M) Fibrosis in renal tissues was determined by Masson's Trichrome staining. [scale bar = 50 μm] (n 6; Mean ± SEM; *P < 0.05).

Funding

This study was supported by the National Natural Science Foundation of China (82273791 to Q.T. and 82000793 to W.L.) and the Key Research Project of Wenzhou City, China (ZY2021021 to Y.W.).

CRediT authorship contribution statement

Guang Liang, Wu Luo, and Ping Huang contributed to the literature search and study design. Guang Liang, Minxiu Wang, and Yi Wang participated in the drafting of the article. Minxiu Wang, Qianhui Zhang, Shuaijie Lou, Leiming Jin, Weiqi Wu, and Qidong Tang carried out the experiments. Gaojun Wu and Xiaohong Long revised the manuscript. Qidong Tang and Wu Luo contributed to data collection and analysis.

Declaration of Competing Interest

The authors declare that they have no conflict of interest.

Data Availability

Data will be made available on request.

Appendix A. Supporting information

Supplementary data associated with this article can be found in the online version at doi:10.1016/j.biopha.2023.115660.

References

[1] G. Tang, S. Li, C. Zhang, H. Chen, N. Wang, Y. Feng, Clinical efficacies, underlying mechanisms and molecular targets of Chinese medicines for diabetic nephropathy treatment and management, Acta Pharm. Sin. B 11 (9) (2021) 2749–2767.
[2] R.A. DeFronzo, W.B. Reeves, A.S. Awad, Pathophysiology of diabetic kidney disease: impact of SGLT2 inhibitors, Nat. Rev. Nephrol. 17 (5) (2021) 319–334.
[3] R. Xue, D. Gui, L. Zheng, R. Zhai, F. Wang, N. Wang, Mechanistic insight and management of diabetic nephropathy: recent progress and future perspective, J. Diabetes Res. 2017 (2017) 1839809.
[4] K. Reidy, H.M. Kang, T. Hostetter, K. Susztak, Molecular mechanisms of diabetic kidney disease, J. Clin. Invest 124 (6) (2014) 2333–2340.
[5] M. Lin, W.H. Yiu, H.J. Wu, L.Y. Chan, J.C. Leung, W.S. Au, K.W. Chan, K.N. Lai, S. C. Tang, Toll-like receptor 4 promotes tubular inflammation in diabetic nephropathy, J. Am. Soc. Nephrol. 23 (1) (2012) 86–102.
[6] C.Q.F. Klessens, M. Zandbergen, R. Wolterbeek, J.A. Bruijn, T.J. Rabelink, I. M. Bajema, I.J. DHT, Macrophages in diabetic nephropathy in patients with type 2 diabetes, Nephrol. Dial. Transpl. 32 (8) (2017) 1322–1329.
[7] J. Ma, S.J. Chadban, C.Y. Zhao, X. Chen, T. Kwan, U. Panchapakesan, C.A. Pollock, H. Wu, TLR4 activation promotes podocyte injury and interstitial fibrosis in diabetic nephropathy, PLoS One 9 (5) (2014), e97985.
[8] I. Jialal, A.M. Major, S. Devaraj, Global Toll-like receptor 4 knockout results in decreased renal inflammation, fibrosis and podocytopathy, J. Diabetes Complicat. 28 (6) (2014) 755–761.
[9] J. Ma, H. Wu, C.Y. Zhao, U. Panchapakesan, C. Pollock, S.J. Chadban, Requirement for TLR2 in the development of albuminuria, inflammation and fibrosis in experimental diabetic nephropathy, Int J. Clin. Exp. Pathol. 7 (2) (2014) 481–495.
[10] K.A. Fitzgerald, J.C. Kagan, Toll-like receptors and the control of immunity, Cell 180 (6) (2020) 1044–1066.
[11] Y. Xu, X. Tao, B. Shen, T. Horng, R. Medzhitov, J.L. Manley, L. Tong, Structural basis for signal transduction by the Toll/interleukin-1 receptor domains, Nature 408 (6808) (2000) 111–115.
[12] B.S. Park, D.H. Song, H.M. Kim, B.S. Choi, H. Lee, J.O. Lee, The structural basis of lipopolysaccharide recognition by the TLR4-MD-2 complex, Nature 458 (7242) (2009) 1191–1195.
[13] Y. Wang, W. Luo, J. Han, Z.A. Khan, Q. Fang, Y. Jin, X. Chen, Y. Zhang, M. Wang, J. Qian, W. Huang, H. Lum, G. Wu, G. Liang, MD2 activation by direct AGE interaction drives inflammatory diabetic cardiomyopathy, Nat. Commun. 11 (1) (2020) 2148.
[14] Y. Wang, Q. Fang, Y. Jin, Z. Liu, C. Zou, W. Yu, W. Li, X. Shan, R. Chen, Z. Khan, G. Liang, Blockade of myeloid differentiation 2 attenuates diabetic nephropathy by reducing activation of the renin-angiotensin system in mouse kidneys, Br. J. Pharm. 176 (14) (2019) 2642–2657.
[15] W. Zhu, M. Wang, L. Jin, B. Yang, B. Bai, R.N. Mutsinze, W. Zuo, N. Chattipakorn, J.Y. Huh, G. Liang, Y. Wang, Licochalcone A protects against LPS-induced inflammation and acute lung injury by directly binding with myeloid differentiation factor 2 (MD2), Br. J. Pharm. 180 (8) (2023) 1114–1131.
[16] Y. Yang, C. Han, Y. Sheng, J. Wang, X. Zhou, W. Li, L. Guo, S. Ruan, The mechanism of aureusidin in suppressing inflammatory response in acute liver injury by regulating MD2, Front. Pharm. 11 (2020), 570776.
[17] X. Wang, C. Lin, S. Wu, T. Zhang, Y. Wang, Y. Jiang, X. Wang, Cannabidivarin alleviates neuroinflammation by targeting TLR4 co-receptor MD2 and improves morphine-mediated analgesia, Front. Immunol. 13 (2022), 929222.
[18] Y. Zhang, T. Xu, Z. Pan, X. Ge, C. Sun, C. Lu, H. Chen, Z. Xiao, B. Zhang, Y. Dai, G. Liang, Shikonin inhibits myeloid differentiation protein 2 to prevent LPS-induced acute lung injury, Br. J. Pharm. 175 (5) (2018) 840–854.
[19] Z. Wang, G. Chen, L. Chen, X. Liu, W. Fu, Y. Zhang, C. Li, G. Liang, Y. Cai, Insights into the binding mode of curcumin to MD-2: studies from molecular docking, molecular dynamics simulations and experimental assessments, Mol. Biosyst. 11 (7) (2015) 1933–1938.
[20] W. Luo, L.B. Yang, C.C. Qian, B. Ma, G.M. Manjengwa, X.M. Miao, J. Wang, C. H. Hu, B. Jin, L.X. Zhang, C. Zheng, G. Liang, Y. Wang, Flavokawain B alleviates LPS-induced acute lung injury via targeting myeloid differentiation factor 2, Acta Pharm. Sin. 43 (7) (2022) 1758–1768.
[21] L. Yang, W. Luo, Q. Zhang, S. Hong, Y. Wang, A.V. Samorodov, N. Chattipakorn, V. N. Pavlov, G. Liang, Cardamonin inhibits LPS-induced inflammatory responses and prevents acute lung injury by targeting myeloid differentiation factor 2, Phytomedicine 93 (2021), 153785.
[22] A. Heydemann, An overview of murine high fat diet as a model for type 2 diabetes mellitus, J. Diabetes Res. 2016 (2016) 2902351.
[23] T. Ma, X. Li, Y. Zhu, S. Yu, T. Liu, X. Zhang, D. Chen, S. Du, T. Chen, S. Chen, Y. Xu, Q. Fan, Excessive activation of notch signaling in macrophages promote kidney inflammation, fibrosis, and necroptosis, Front. Immunol. 13 (2022), 835879.
[24] J.F. Navarro-Gonzalez, C. Mora-Fernandez, The role of inflammatory cytokines in diabetic nephropathy, J. Am. Soc. Nephrol. 19 (3) (2008) 433–442.
[25] C.Y. Jung, T.H. Yoo, Pathophysiologic mechanisms and potential biomarkers in diabetic kidney disease, Diabetes Metab. J. 46 (2) (2022) 181–197.
[26] P. Calle, G. Hotter, Macrophage phenotype and fibrosis in diabetic nephropathy, Int. J. Mol. Sci. 21 (8) (2020).
[27] G.H. Tesch, Role of macrophages in complications of type 2 diabetes, Clin. Exp. Pharm. Physiol. 34 (10) (2007) 1016–1019.
[28] S.C. Tang, L.Y. Chan, J.C. Leung, A.S. Cheng, K.W. Chan, H.Y. Lan, K.N. Lai, Bradykinin and high glucose promote renal tubular inflammation, Nephrol. Dial. Transpl. 25 (3) (2010) 698–710.
[29] S.C.W. Tang, W.H. Yiu, Innate immunity in diabetic kidney disease, Nat. Rev. Nephrol. 16 (4) (2020) 206–222.
[30] A.C. Chung, H.Y. Lan, Chemokines in renal injury, J. Am. Soc. Nephrol. 22 (5) (2011) 802–809.
[31] M. Mack, M. Yanagita, Origin of myofibroblasts and cellular events triggering fibrosis, Kidney Int. 87 (2) (2015) 297–307.
[32] X.M. Meng, D.J. Nikolic-Paterson, H.Y. Lan, Inflammatory processes in renal fibrosis, Nat. Rev. Nephrol. 10 (9) (2014) 493–503.
[33] J. Wada, H. Makino, Innate immunity in diabetes and diabetic nephropathy, Nat. Rev. Nephrol. 12 (1) (2016) 13–26.
[34] J.C. Leemans, L.M. Butter, W.P. Pulskens, G.J. Teske, N. Claessen, T. van der Poll, S. Florquin, The role of Toll-like receptor 2 in inflammation and fibrosis during progressive renal injury, PLoS One 4 (5) (2009), e5704.
[35] Z. Xu, W. Li, J. Han, C. Zou, W. Huang, W. Yu, X. Shan, H. Lum, X. Li, G. Liang, Angiotensin II induces kidney inflammatory injury and fibrosis through binding to myeloid differentiation protein-2 (MD2), Sci. Rep. 7 (2017) 44911.
[36] D. De, Nardo, Toll-like receptors: activation, signalling and transcriptional modulation, Cytokine 74 (2) (2015) 181–189.
[37] H.J. Sun, S.P. Xiong, X. Cao, L. Cao, M.Y. Zhu, Z.Y. Wu, J.S. Bian, Polysulfide-mediated sulfhydration of SIRT1 prevents diabetic nephropathy by suppressing phosphorylation and acetylation of p65 NF-kappaB and STAT3, Redox Biol. 38 (2021), 101813.
[38] F. Li, Y. Chen, Y. Li, M. Huang, W. Zhao, Geniposide alleviates diabetic nephropathy of mice through AMPK/SIRT1/NF-kappaB pathway, Eur. J. Pharm. 886 (2020), 173449.
[39] X. Xu, L. Zhang, F. Hua, C. Zhang, C. Zhang, X. Mi, N. Qin, J. Wang, A. Zhu, Z. Qin, F. Zhou, FOXM1-activated SIRT4 inhibits NF-kappaB signaling and NLRP3 inflammasome to alleviate kidney injury and podocyte pyroptosis in diabetic nephropathy, Exp. Cell Res. 408 (2) (2021), 112863.
[40] M. Zhang, Y. Chen, M.J. Yang, X.R. Fan, H. Xie, L. Zhang, Y.S. Nie, M. Yan, Celastrol attenuates renal injury in diabetic rats via MAPK/NF-kappaB pathway, Phytother. Res 33 (4) (2019) 1191–1198.
[41] E.J. Lewis, L.G. Hunsicker, W.R. Clarke, T. Berl, M.A. Pohl, J.B. Lewis, E. Ritz, R. C. Atkins, R. Rohde, I. Raz, G. Collaborative Study, Renoprotective effect of the angiotensin-receptor antagonist irbesartan in patients with nephropathy due to type 2 diabetes, N. Engl. J. Med 345 (12) (2001) 851–860.
[42] E.J. Lewis, J.B. Lewis, Treatment of diabetic nephropathy with angiotensin II receptor antagonist, Clin. Exp. Nephrol. 7 (1) (2003) 1–8.
[43] L.M. Ruilope, Renoprotection and renin-angiotensin system blockade in diabetes mellitus, Am. J. Hypertens. 10 (12 Pt 2) (1997) 325S–331S.
[44] M.A. Morsy, G.H. Heeba, M.E. Mahmoud, Ameliorative effect of eprosartan on high-fat diet/streptozotocin-induced early diabetic nephropathy in rats, Eur. J. Pharm. 750 (2015) 90–97.
[45] W. Luo, L. Ye, X.T. Hu, M.H. Wang, M.X. Wang, L.M. Jin, Z.X. Xiao, J.C. Qian, Y. Wang, W. Zuo, L.J. Huang, G. Liang, MD2 deficiency prevents high-fat diet-

induced AMPK suppression and lipid accumulation through regulating TBK1 in non-alcoholic fatty liver disease, Clin. Transl. Med. 12 (3) (2022), e777.
[46] L. Wang, J. Han, P. Shan, S. You, X. Chen, Y. Jin, J. Wang, W. Huang, Y. Wang, G. Liang, MD2 blockage protects obesity-induced vascular remodeling via activating AMPK/Nrf2, Obesity 25 (9) (2017) 1532–1539.
[47] V. Rajamanickam, T. Yan, S. Xu, J. Hui, X. Xu, L. Ren, Z. Liu, G. Liang, O. Wang, Y. Wang, Selective targeting of the TLR4 co-receptor, MD2, prevents colon cancer growth and lung metastasis, Int. J. Biol. Sci. 16 (8) (2020) 1288–1302.